Chapter 4

Results

4.1 Overview

This chapter contains results of inverting synthetic and field seismic data. Both are interesting tests of elastic inversion using nonlinear least squares. The emphasis is placed on the resolution between the P- and S-wave velocity models and the relative resolution of the high- and low-wavenumber components of the velocity models.

This thesis concentrates on using direct P- and S-waves and P-P and P-S primary reflections to resolve the velocities in the non near-surface parts of the Earth model. Consequently, an absorbing boundary condition was used at the Earth's surface to avoid the generation of Rayleigh waves that would only help resolve the near surface at the expense of increased CPU. Note that the inversion should not be adversely affected by the use of an absorbing rather than a more realistic free surface boundary condition because the P-P and P-S reflection amplitudes are almost the same in both cases (Appendix A).

The shot and back-propagated residual wavefields required by the inversion were computed using the method finite differences described by Mora (1986) to simulate 2D waves in an isotropic elastic medium. The full two-way elastic wave equation was used so both wavefields contain up and downgoing waves. This is a crucial element in the inversion because it enables the low wavenumbers to be resolved as will be shown mathematically in the next chapter. The reason is that the two-way wave equation can model reflections and it is the traveltime shapes of these events that provides the low-wavenumber velocity information.

Synthetic data were generated using the same finite difference method as was used in

the inversion. Inversions of both two- and single-component synthetic data illustrate the importance of P-S and S-S reflections in resolving the S-wave velocity. The effect of adding Gaussian noise is also examined.

Finally, the consequence of reflected waves on the inversion results versus that of transmitted waves is examined. This is done by comparing results of an inversion of shot gathers (reflection data) with results of an inversion including VSP's (transmission data).

The inversion of field data is far more challenging than synthetic data inversions because of inadequacies in the assumption of the 2D elastic wave equation to simulate seismic waves. A two component shot gather containing P-P and P-S primary reflections has been inverted and the results show that, despite inadequacies in the modeling theory, the P- and S-wave velocities can be resolved.

4.2 Noisy diffractions

Noise contaminated diffractions were inverted to test the resolution of the P- and S-wave velocities and densities of the inversion result.

The diffractor model is shown in Figure 4.1 and contains twelve diffracting points at different depths. Three diffractors are perturbations in P-wave velocity only, three are perturbations S-wave velocity only, three are in density only and three are perturbations in all three properties. The perturbations were -15% relative to the background properties of $\alpha = 3$ km/s, $\beta = 1.7$ km/s and $\rho = 2gm/cm^3$. This model was chosen to study the change in resolution between the different parameters as depth increases and consequently the effective angular aperture decreases. Angles of incidence vary from about 50 degrees for the shallower diffractors to 30 degrees for the deeper diffractors.

A synthetic two-component shot gather was generated from the diffractor model using the method of elastic finite differences and 50−100% band-limited Gaussian noise was added (Figure 4.2). The data were computed by applying a vertical force on the surface of the Earth at the center of the model. The source time function was band-limited being a second derivative of a Gaussian curve with a fundamental frequency of 20 Hz.

An inversion was done assuming the source wavelet and background medium were known. The results after one and seven iterations are plotted in Figures 4.3 through 4.5.

The results have good spatial resolution of the diffracting points, good resolution between the P- and S-wave velocity and poor resolution between P-wave velocity and density.

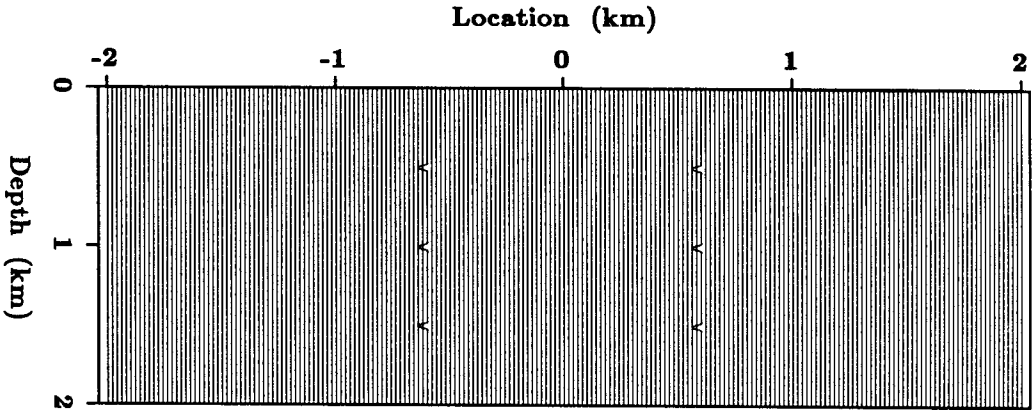

Figure 4.1: (a). P-wave diffractor velocity model relative to a homogeneous background.

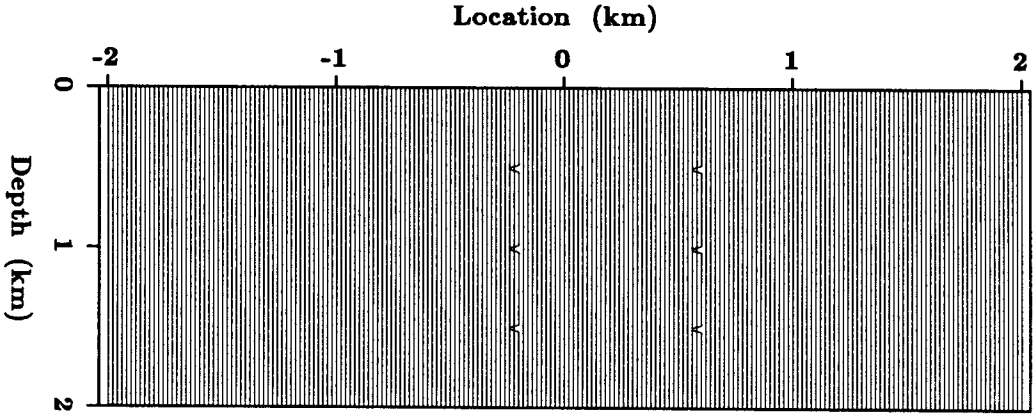

Figure 4.1: (b). S-wave diffractor velocity model relative to a homogeneous background.

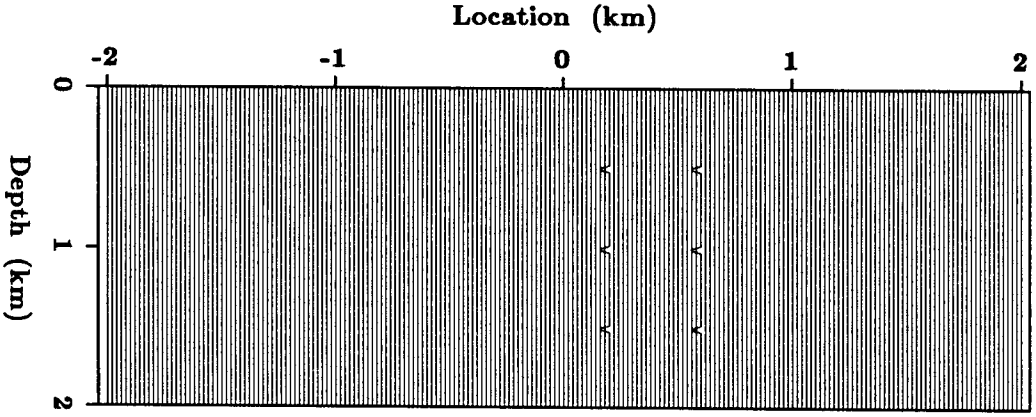

Figure 4.1: (c). Density diffractor model relative to a homogeneous background.

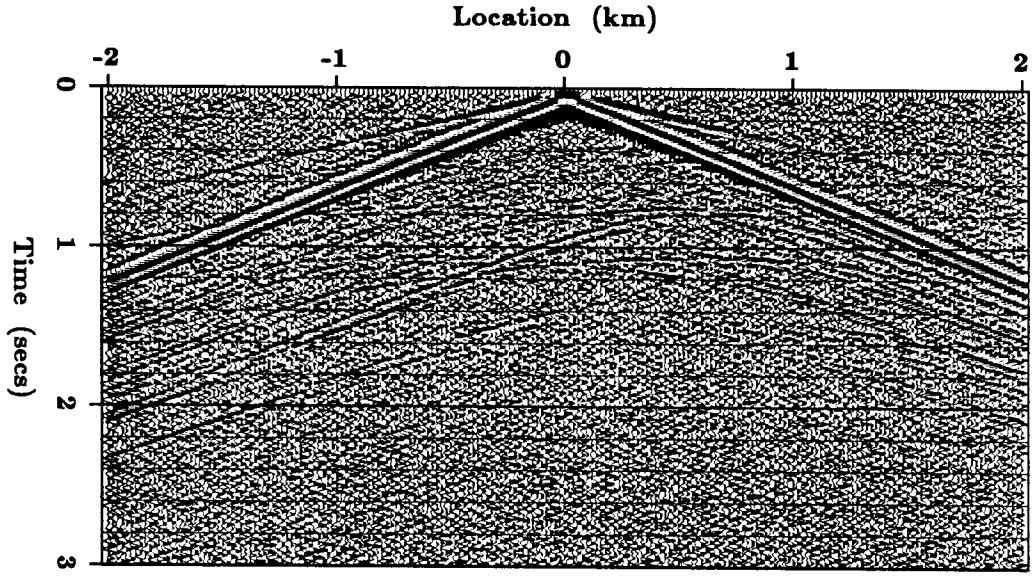

Figure 4.2: (a). Vertical component shot gather for the diffractor model.

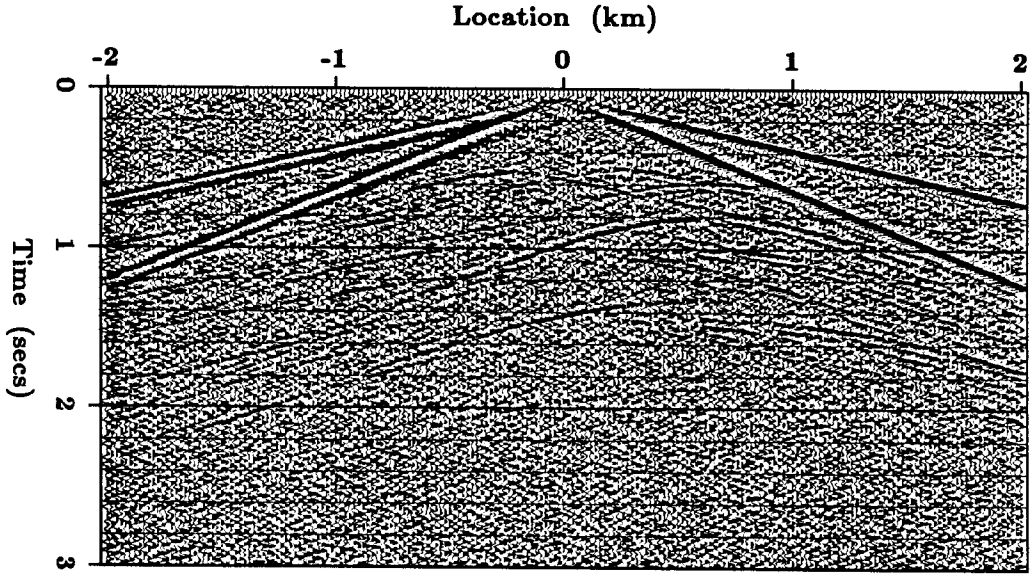

Figure 4.2: (b). Horizontal component shot gather for the diffractor model.

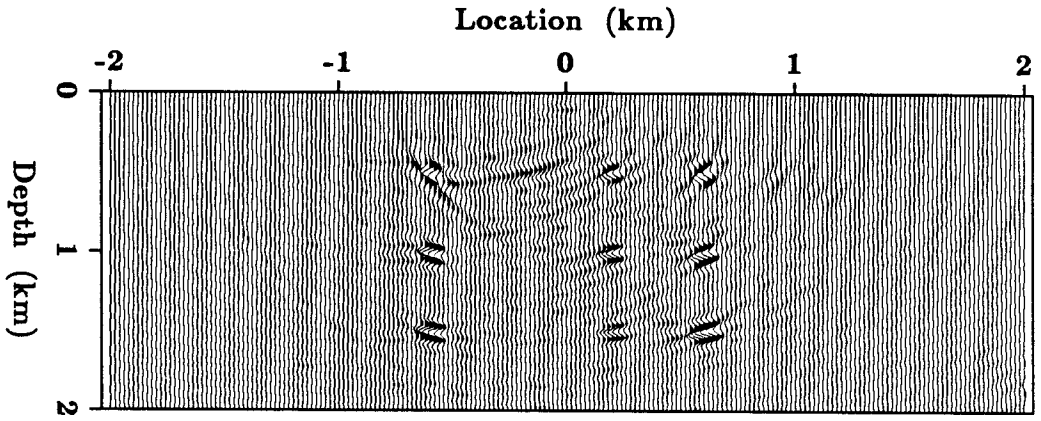

Figure 4.3: (a). One iteration P-wave velocity inversion result of diffraction data.

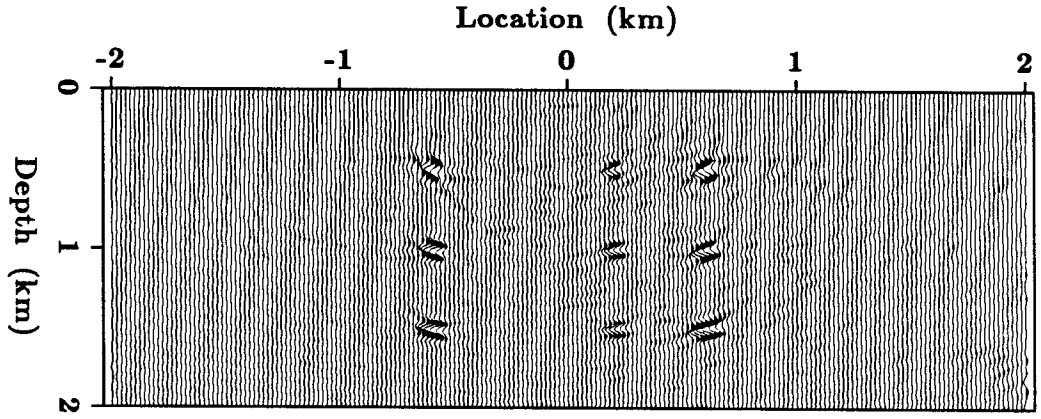

Figure 4.3: (b). Seven iteration P-wave velocity inversion result of diffraction data.

The noise contamination in the velocity and density solution is lower than expected considering the problem is overdetermined by a factor of 2.75 and Figure 4.2 suggests the signal to noise ratio in the data is about 2:1 implying a signal to noise level of about 3:1 in the solution. The circular artifacts near the edges of the model, especially in the S-wave velocity solution, occur because of smaller effective angular aperture resulting in a poorer resolution around the edges (c.f. migration which will resolve a point diffractor when there are many sources and receivers but will yield an ellipse if there is only one source and one receiver). The effect of iterations is to correct the relative amplitudes of the perturbations and to decrease the relative size of artifacts (circular migration-like smiles centered on the diffractors). A side effect of the iterations is to amplify the circular artifacts in the poorly resolved edge regions of the model. This would not occur if the inversion used several shot gathers because the velocities and density near the edges would be better resolved.

The magnitudes of perturbations obtained in the inversion are only 25% of the true values. This is because of the band limitation of the seismic source leading to a band limited solution of smaller magnitude.

The mismatch between the data computed from the inversion result (termed the "synthetic data") and the synthetic data corresponding to the true model (termed the "true data") after seven iterations is shown in Figure 4.6. It is mainly Gaussian noise that cannot be matched to elastic waves. The coherent energy that exists near the bottom of the time axis is because of truncation of the circular artifacts in the S-wave velocity solution at the edge of the model.

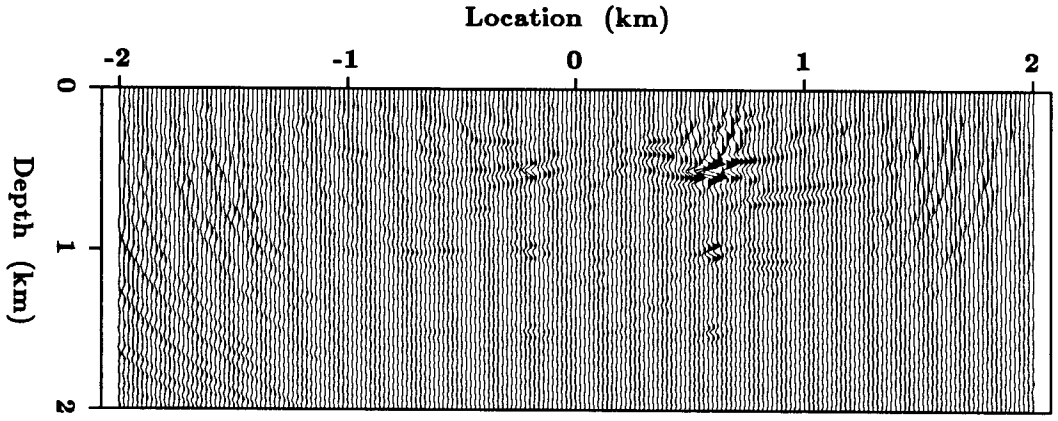

Figure 4.4: (a). One iteration S-wave velocity inversion result of diffraction data.

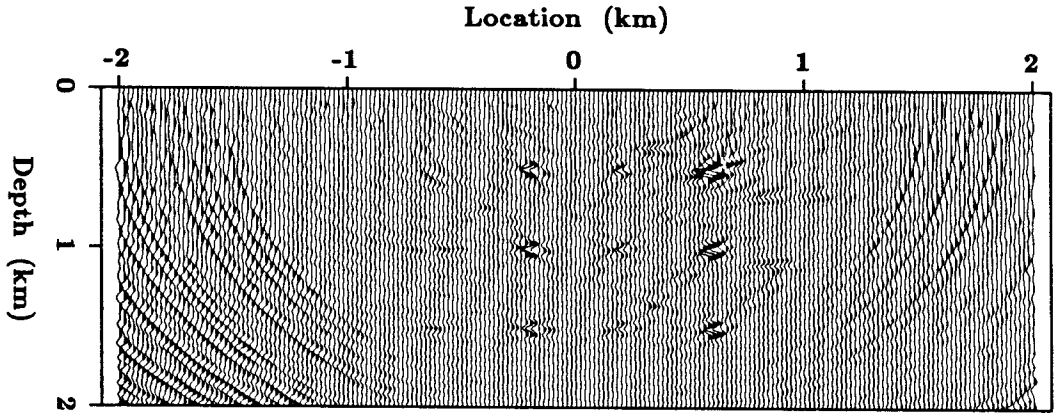

Figure 4.4: (b). Seven iteration S-wave velocity inversion result of diffraction data.

The inversion shows that P- and S-wave velocity can be resolved from one another using ideal Gaussian noise contaminated data that contains P-P and P-S events. However, density cannot be easily resolved from P-wave velocity and is therefore not an important

parameter relative to P- and S-wave velocity (hence, the real data inversion solves only for the P- and S-wave velocity models).

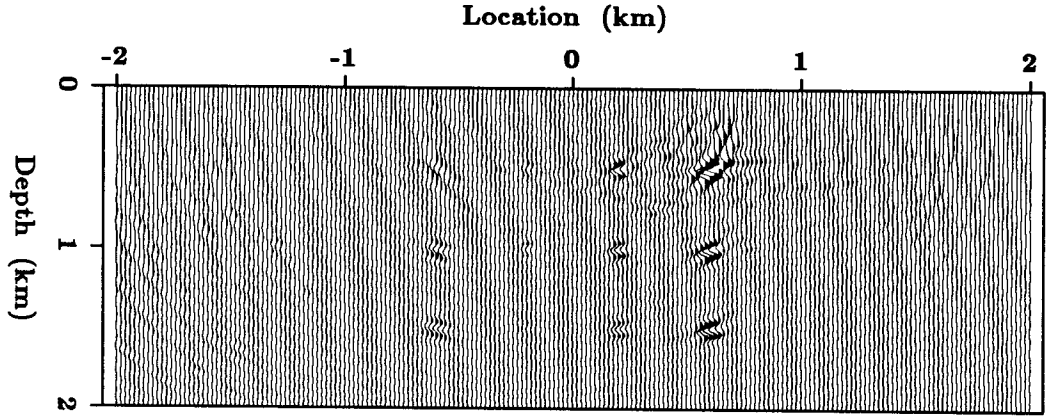

Figure 4.5: (a). One iteration density inversion result of diffraction data.

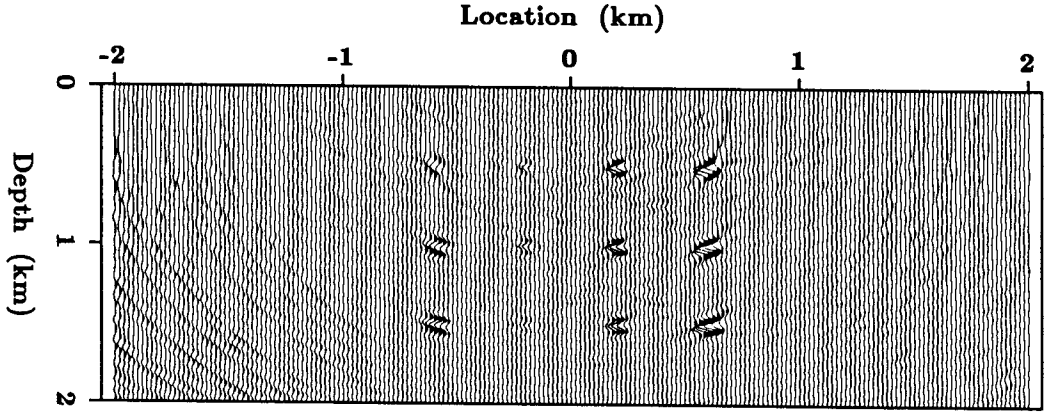

Figure 4.5: (b). Seven iteration density inversion result of diffraction data.

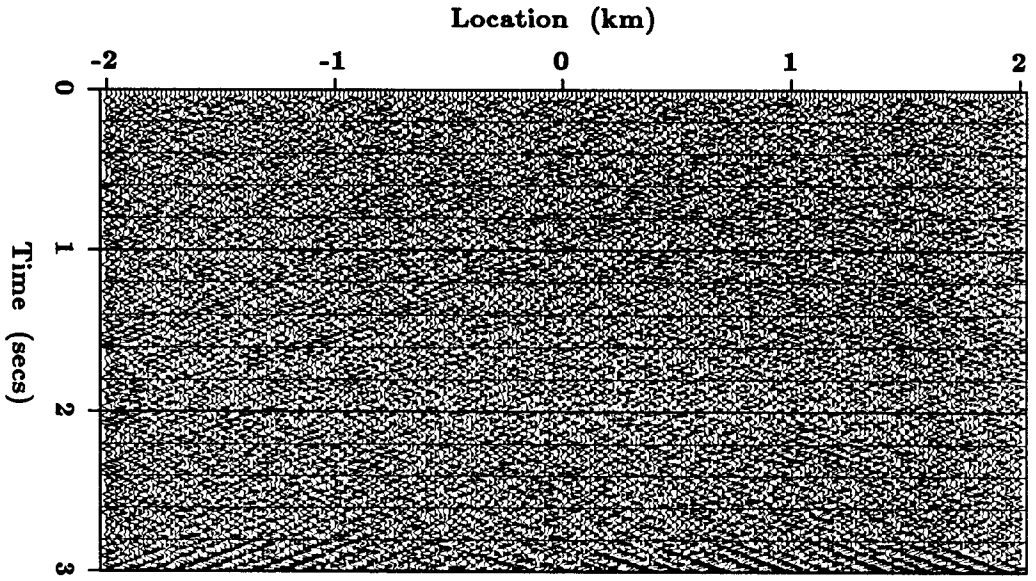

Figure 4.6: (a). Vertical component mismatch after inverting the diffraction data.

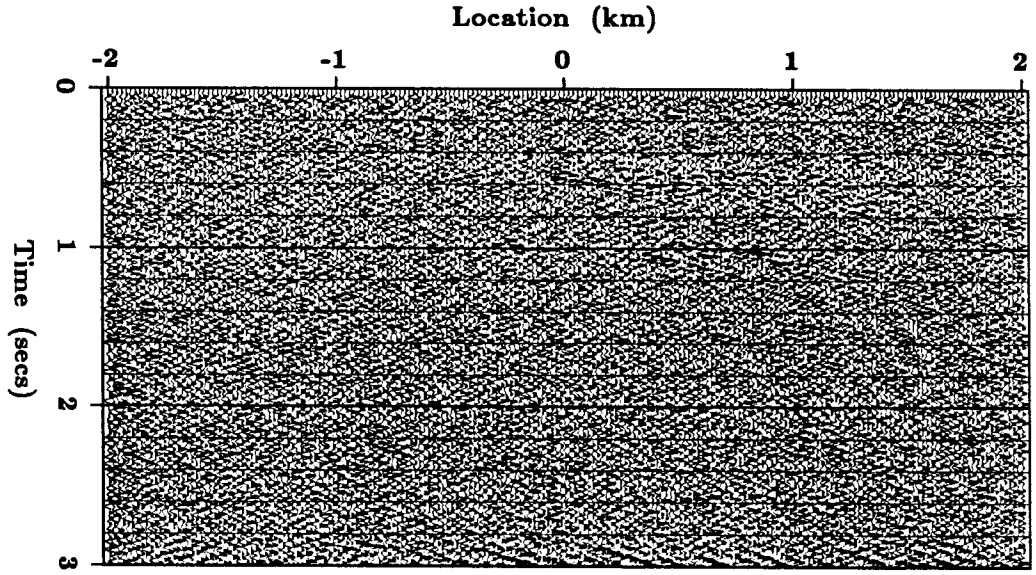

Figure 4.6: (b). Horizontal component mismatch after inverting the diffraction data.

4.3 Single component data

An inversion was done of noise-free vertical-component data to determine if the strong P-S, S-P and S-S events present in the previous example were necessary for a good determination of the S-wave velocity. This is an important test because most surveys routinely performed today measure only one component of ground displacement and hence mainly P-P events. Will single component data resolve the S-wave velocity adequately?

This test used exactly the same parameters as in the noisy diffractors example except that only the noise free vertical component gather was used in the inversion. The results after one and seven iterations is shown in Figures 4.7 through 4.9.

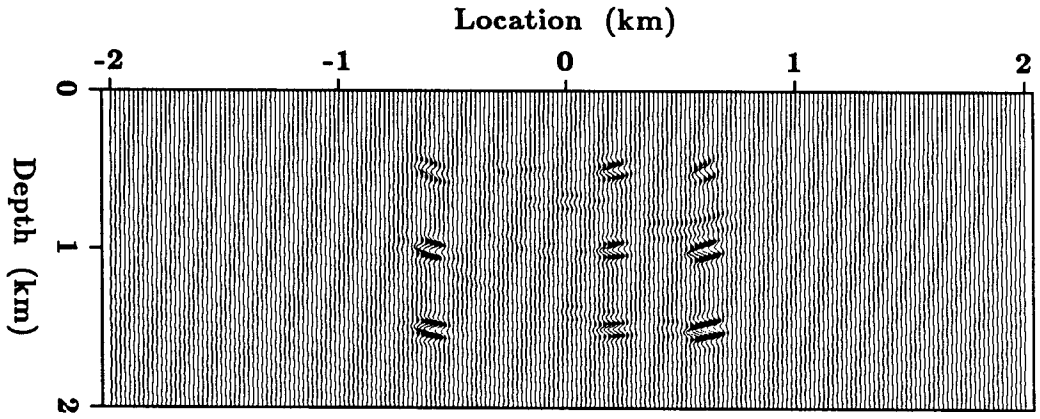

Figure 4.7: (a). One iteration P-wave velocity inversion result using the vertical component diffraction data.

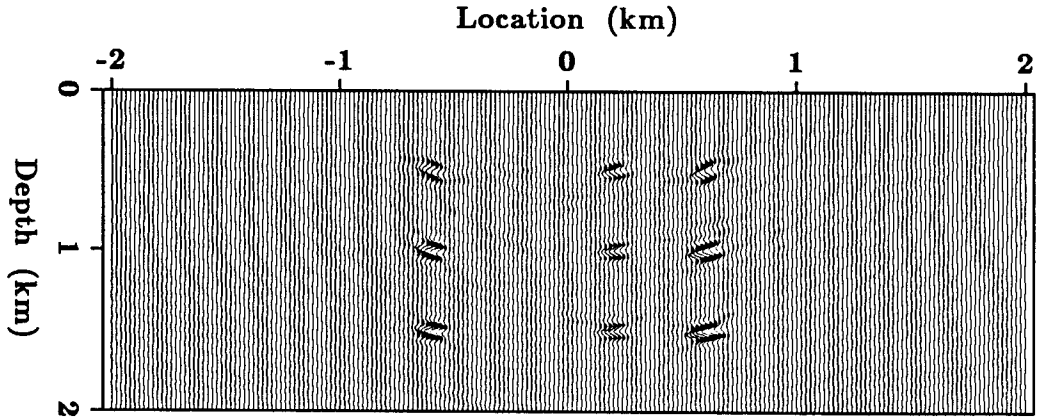

Figure 4.7: (b). Seven iteration P-wave velocity inversion result using the vertical component diffraction data.

Figures 4.7 through 4.9 show that relative to the two-component example (noisy diffractions), the S-wave velocity has a poorer resolution after the first iteration but the improvement with iteration is more significant. The first iteration S-wave velocity initially contains strong circular finite aperture artifacts centered on the diffractors and these become more dominant with depth. As the iterations proceed, these artifacts decrease in magnitude relative to the diffraction point.

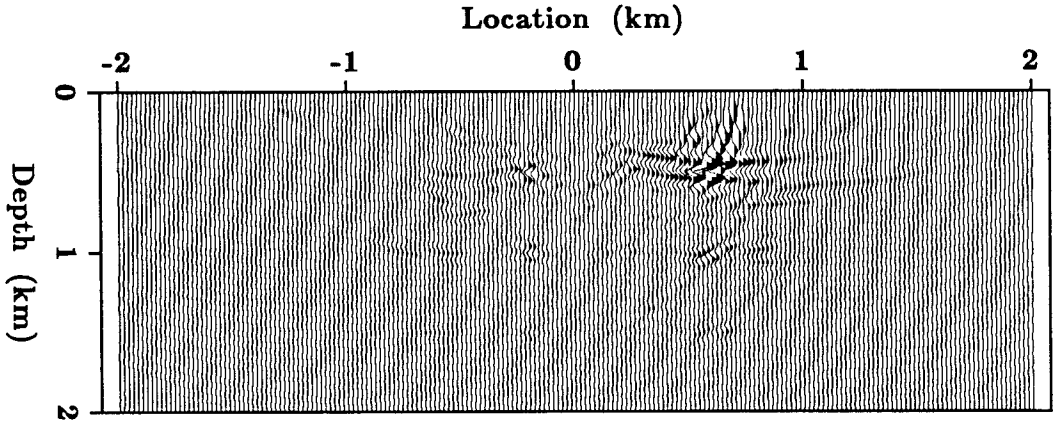

Figure 4.8: (a). One iteration S-wave velocity inversion result using the vertical component diffraction data.

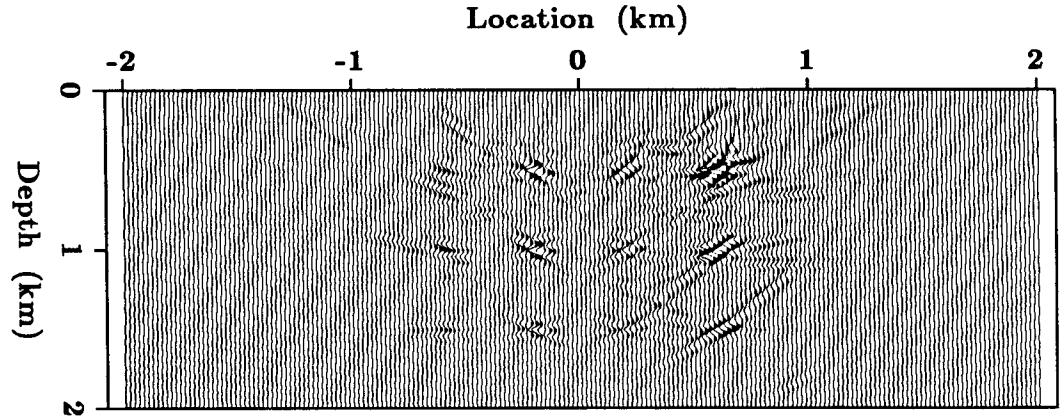

Figure 4.8: (b). Seven iteration S-wave velocity inversion result using the vertical component diffraction data.

As expected, the resolution of the S-wave velocity is poorer here than for the two-component inversion. Also, the resolution of the S-wave velocity decreases with depth indicating the importance of angular aperture. When the aperture is large, there are more S-waves recorded even on vertical component data so the resolution of the S-wave velocity is better.

This inversion test shows the importance of P-S, S-P and S-S events for resolving the S-wave velocity. Of course, amplitude as a function of incidence angle of P-P events helps to constrain the S-wave velocity too, but this is a second order effect in comparison to the presence of mode conversions and would probably be swamped by noise in realistic examples. Therefore, the results here imply that P-S and S-S events such as are found on either wide offset seismic experiments or multi-component data are required to resolve the S-wave velocity.

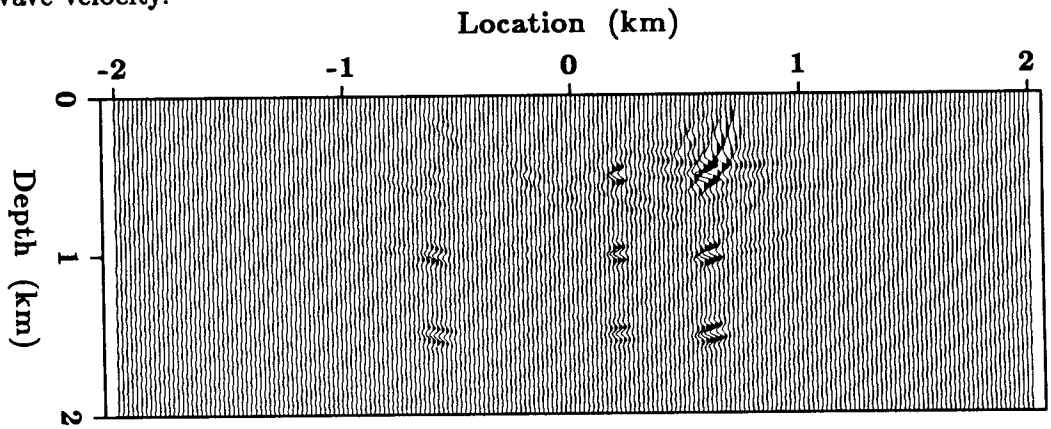

Figure 4.9: (a). One iteration density inversion result using the vertical component diffraction data.

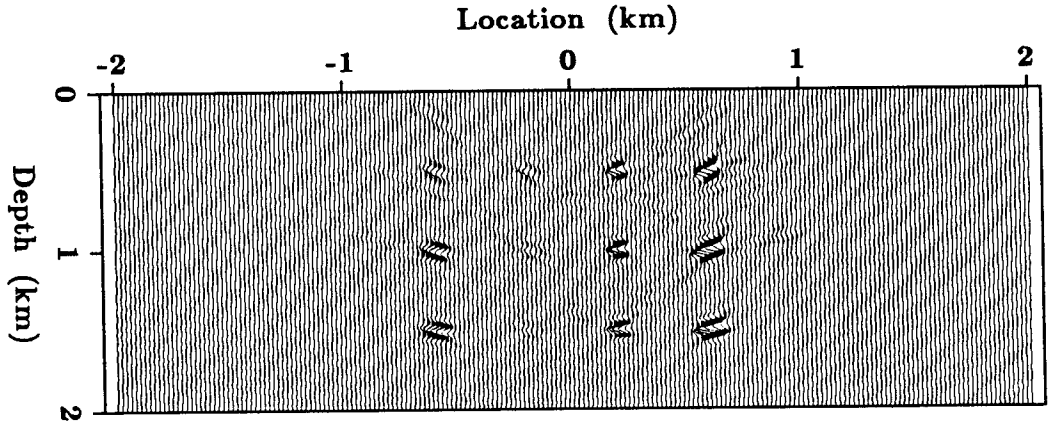

Figure 4.9: (b). Seven iteration density inversion result using the vertical component diffraction data.

4.4 Reflection seismic data

This section shows an inversion of synthetic reflection data generated from a more realistic model to discover how well the P- and S-wave velocity models are resolved when the data are complex. Also, by comparison of the results of this section with those of the next section where VSP's have additionally been included in the data set, I will show influence of transmitted waves on the inversion results.

A model consisting of several gross layers, a deep fault block with a gas pocket and a shallower limestone reef was specified (Figure 4.10).

Each of the gross layers have random fine layer structures within them to simulate sedimentary sequences. Although the gross layer boundaries match, there is not always a strong correlation between the P-wave velocity, S-wave velocity and density within the layers. For example, there is a flat gas-water contact at the top of the deep fault block which can be seen on the P-wave velocity model and density model but *not* on the S-wave velocity model (because the kind of fluid in the pore space does not affect the S-wave velocity). Also the semicircular reef has a high P-wave velocity but low S-wave velocity whereas most layers tend to have an overall correlation between the P- and S-wave interval velocities (i.e. $\beta/\alpha \approx .56$). Similarly, the density within the layers does not always correlate with P- or S-wave velocity as in the layer below the semicircular reef which has a low density but high P- and S-wave velocities.

Nine shot gathers were generated using a fixed receiver array spanning the model and a vertical component forcing function (see Figure 4.11). The time dependence of the source was a fourth derivative of a Gaussian curve with a similar band limitation as typical seismic wavelets in reflection seismology. This source was chosen because the band-limited nature of real seismic wavelets is usually the bane of seismic inversions. Most other inversion methods, like migration methods, obtain only the high-wavenumber components of the velocities and are consequently unconvincing. Because my inversion algorithm is based on matching the seismic amplitude data, I expect to obtain both high and low wavenumbers in velocity. Reflection amplitudes should resolve the sharp discontinuities (high wavenumbers) while reflection hyperbola shapes should resolve the interval velocities (low wavenumbers).

An inversion of the nine shot gathers was performed using a smoothly varying initial model consisting of a linear variation of velocity and density with depth. A preconditioning

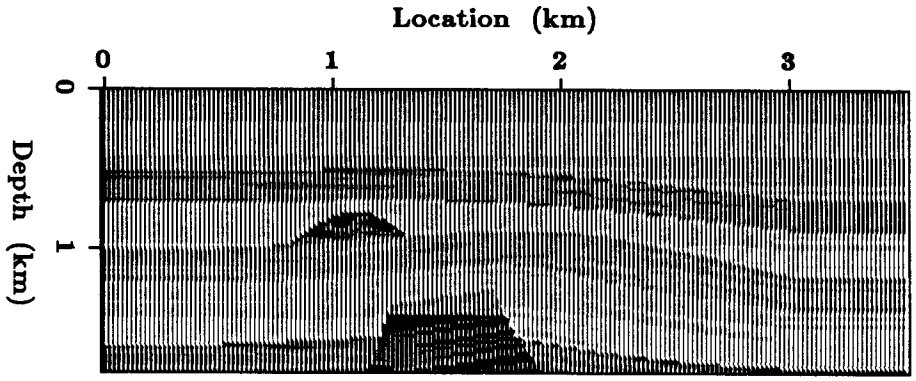

Figure 4.10: (a). P-wave velocity relative to a linear background function for the horst/reef model.

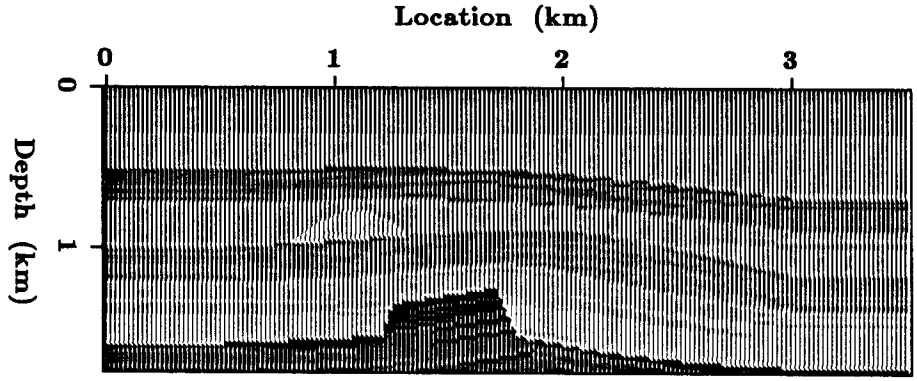

Figure 4.10: (b). S-wave velocity relative to a linear background function for the horst/reef model.

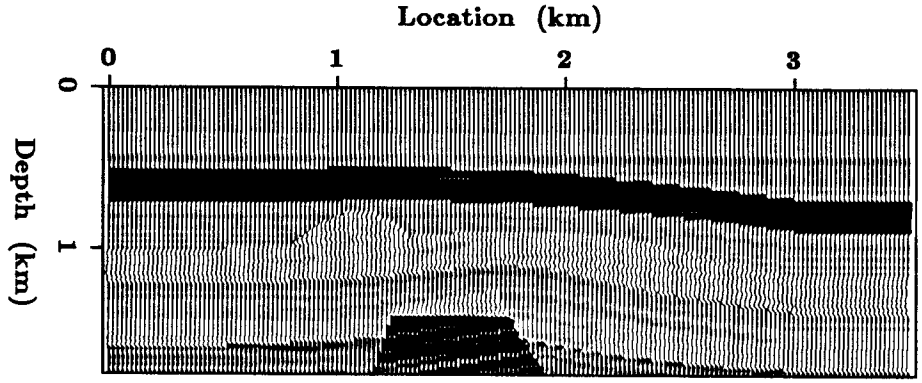

Figure 4.10: (c). Density model relative to a linear background function for the horst/reef model.

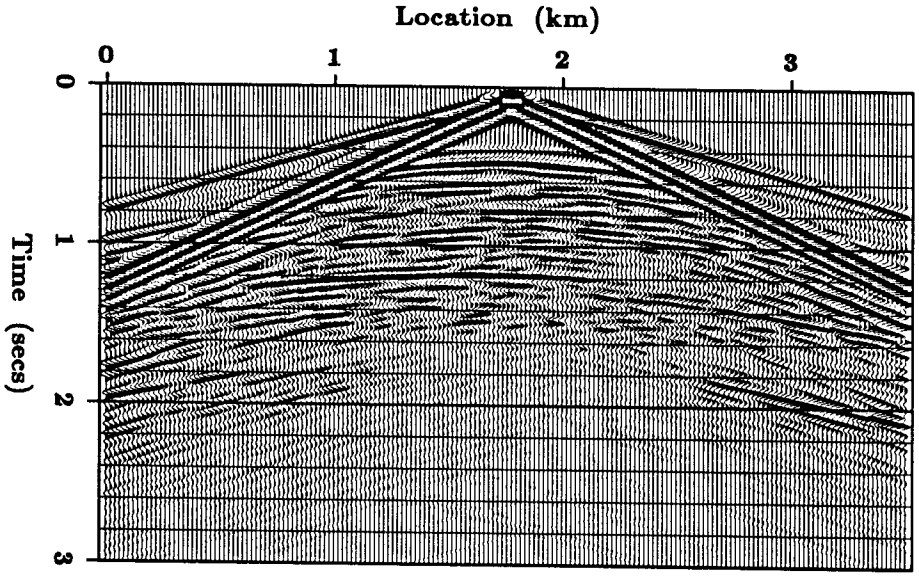

Figure 4.11: (a). A vertical component shot gather for the horst/reef model.

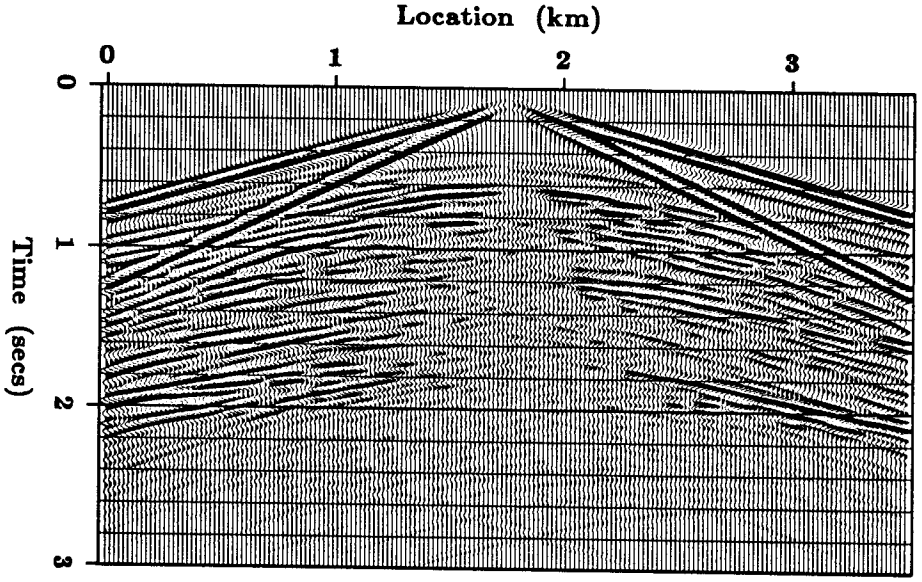

Figure 4.11: (b). A horizontal component shot gather for the horst/reef model.

was used that spatially equalized the perturbations and allowed for the scale differences between the three parameters, P- and S-wave velocity and density. The spatial equalization is equivalent to the assumption that the statistics of the Earth properties are spatially invariant. Hence, gradual changes in the magnitude of the gradient are caused by non-geological factors such as different effective apertures.

The inversion results after one and ten iterations are shown in Figures 4.12 through 4.14 with the filtered true model for comparison. The results are clearly band limited versions of the true model and look similar to what would be expected from an elastic migration that simultaneously accounts for P-P, P-S, S-P and S-S events. However, the P- and S-wave velocities are well resolved from one another after ten iterations as is evidenced by the presence of the gas/water contact at the top of the fault block in the P-wave velocity solution and lack of this feature in the S-wave velocity. By comparison, the elastic migration results or first iteration results are noisy and have not resolved between the P- and S-wave velocities (refer also to the chapter on elastic inverse theory).

A velocity log through the reef is graphed in Figure 4.15 to show the magnitude of the velocity and density perturbations in the solution. The perturbations are too small after the first iteration but build up somewhat after ten iterations. However, the solution is band limited with about the same spectrum as the source wavelet. While the low wavenumbers have built up slightly with iteration (Figure 4.16), they are still almost absent especially in comparison with the true spectrum (Figure 4.17). Why haven't the hyperbola shapes resolved the interval velocities? It must be that more iterations are required to resolve the low wavenumbers. This is examined in detail in the next chapter where I show how to extend the algorithm to obtain equal rates of convergence for the high and low wavenumbers.

The mismatch between data computed from the ten iteration inversion result (termed the "synthetic data") and the synthetic data computed from the true model (termed the "true data") is shown in Figure 4.18. The remaining mismatches are partially caused by incorrect hyperbola shapes that would disappear if enough iterations were performed. Actually, since the velocity perturbations are small in this example, it may even be impossible to resolve a better interval velocity model than the starting model. The reason is that the initial model already accounts for hyperbola shapes well enough that the hyperbolic mismatch will probably be below any realistic noise level.

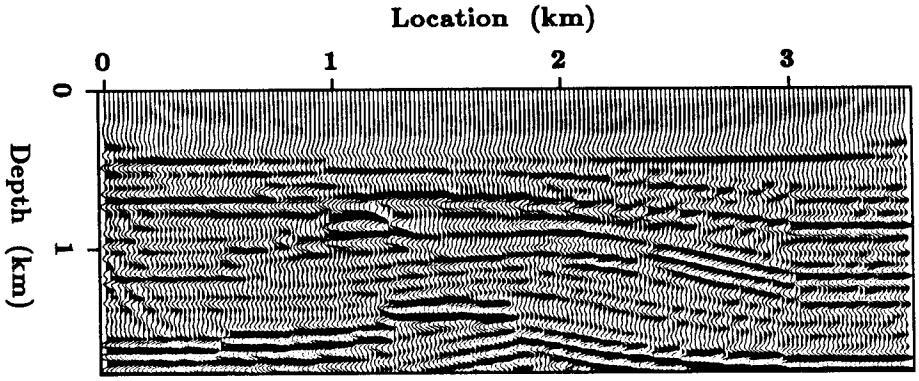

Figure 4.12: (a). One iteration P-wave velocity inversion result using the horst/reef reflection data.

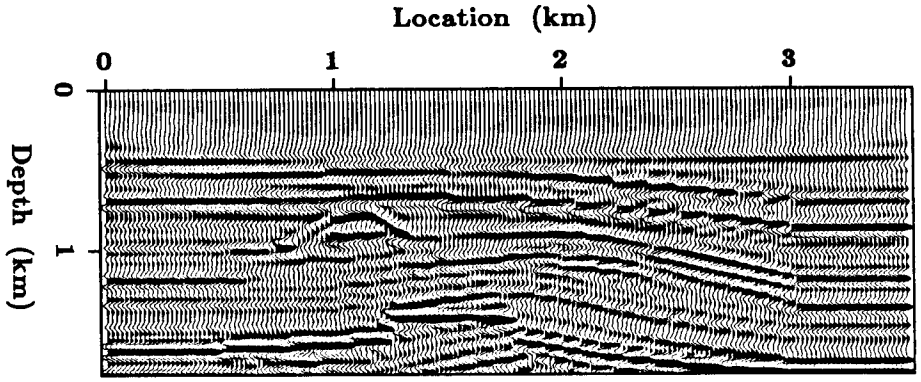

Figure 4.12: (b). Ten iteration P-wave velocity inversion result using the horst/reef reflection data.

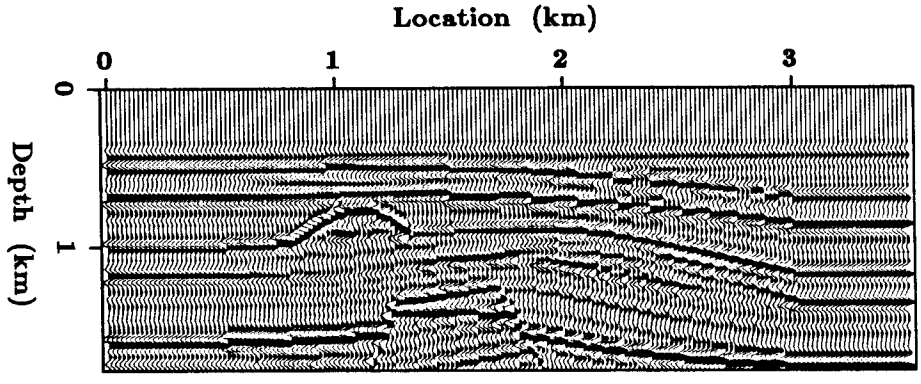

Figure 4.12: (c). Filtered version of the P-wave velocity for the horst/reef model.

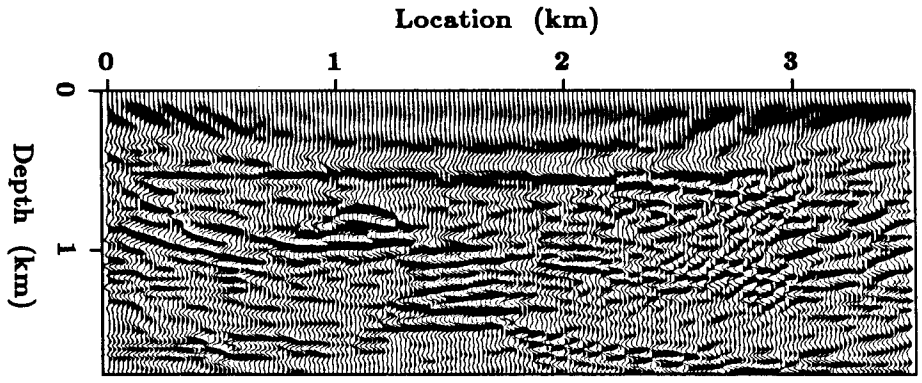

Figure 4.13: (a). One iteration S-wave velocity inversion result using the horst/reef reflection data.

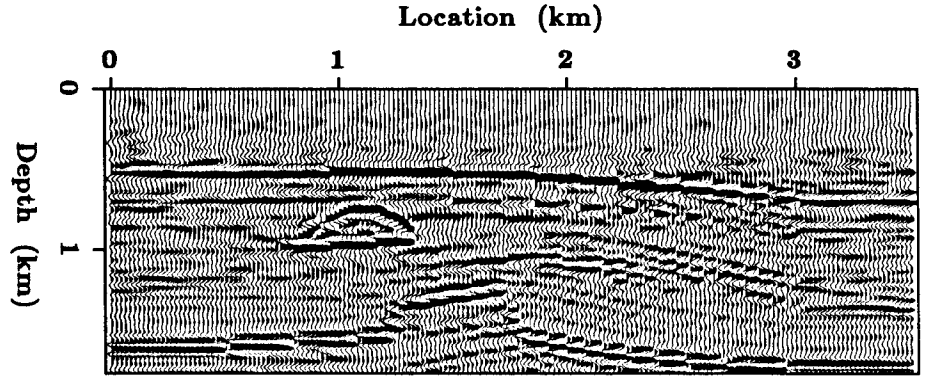

Figure 4.13: (b). Ten iteration S-wave velocity inversion result using the horst/reef reflection data.

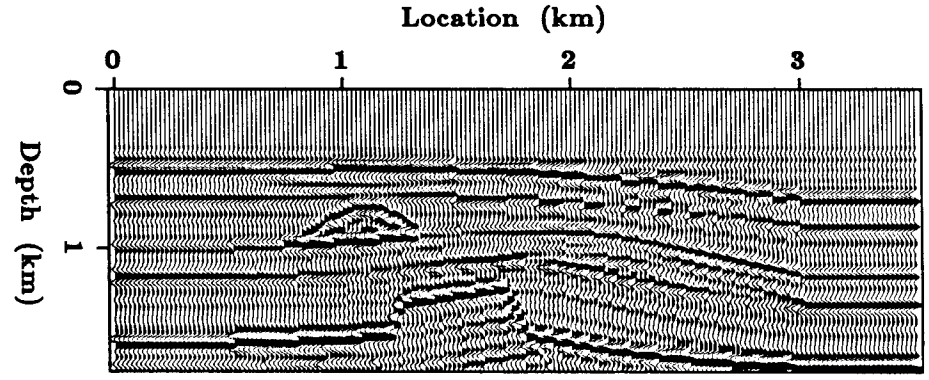

Figure 4.13: (c). Filtered version of the S-wave velocity for the horst/reef model.

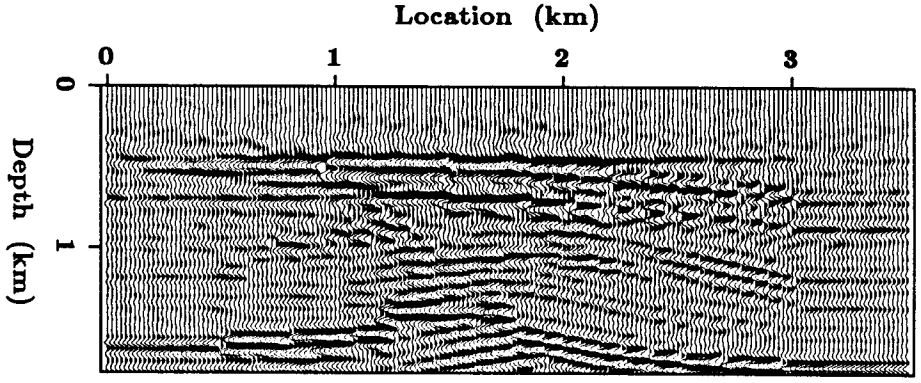

Figure 4.14: (a). One iteration density inversion result using the horst/reef reflection data.

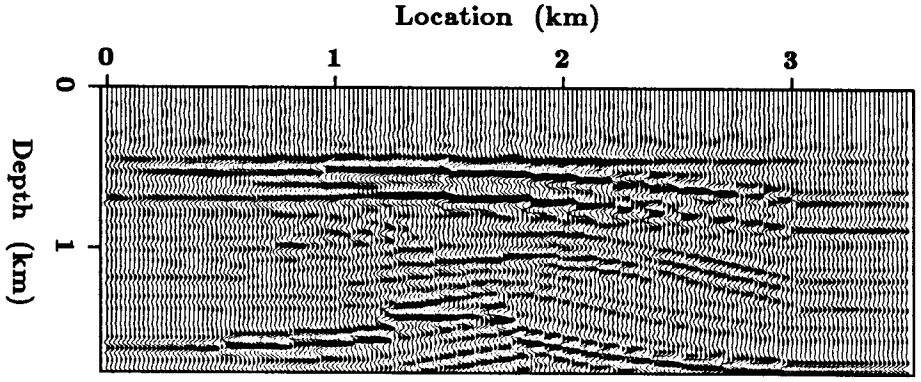

Figure 4.14: (b). Ten iteration density inversion result using the horst/reef reflection data.

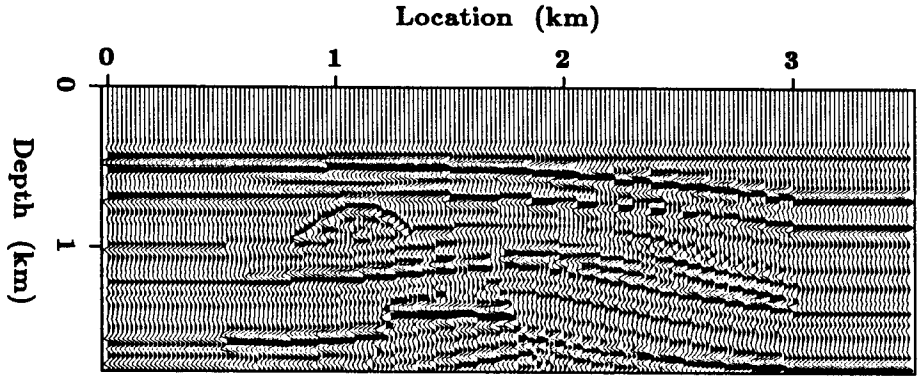

Figure 4.14: (c). Filtered version of the density for the horst/reef model.

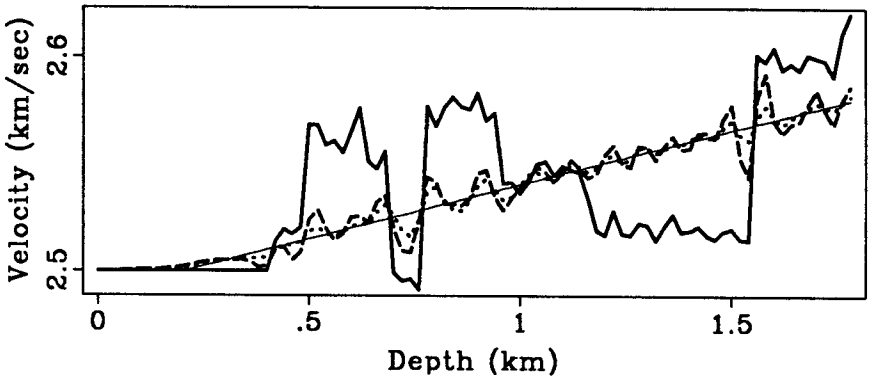

Figure 4.15: (a). P-wave velocity log through the reef: true model (bold line), initial model (fine line), one iteration result (dotted line) and ten iteration result (broken line).

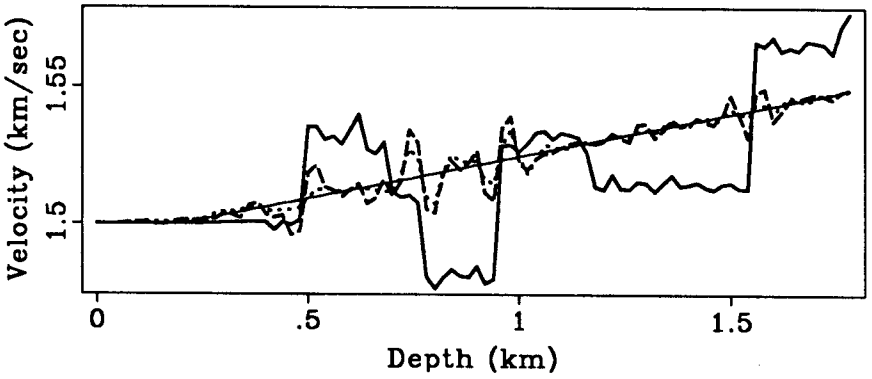

Figure 4.15: (b). S-wave velocity log through the reef: true model (bold line), initial model (fine line), one iteration result (dotted line) and ten iteration result (broken line).

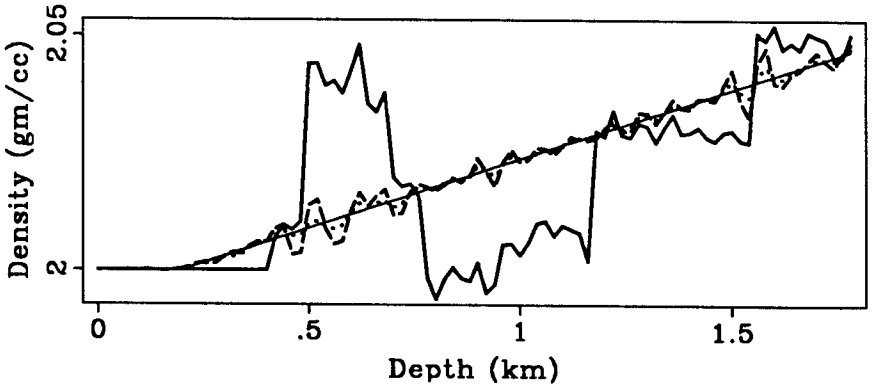

Figure 4.15: (c). Density log through the reef: true model (bold line), initial model (fine line), one iteration result (dotted line) and ten iteration result (broken line).

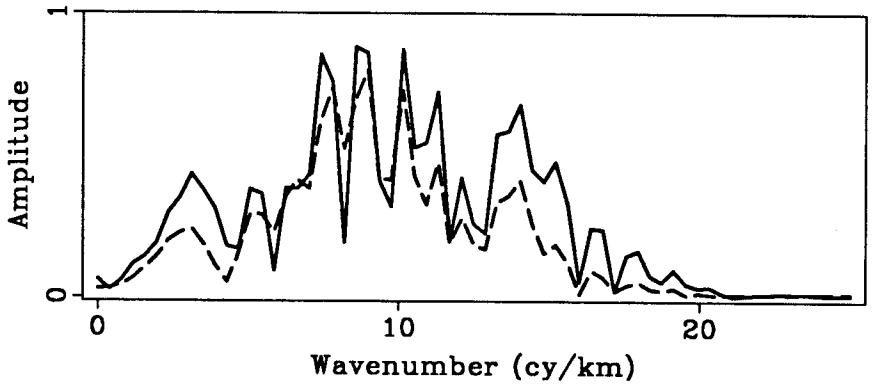

Figure 4.16: Vertical wavenumber spectrum of the P-wave velocity log through the reef obtained by the inversion shown in Figure 4.15 (a): after one iteration (broken line) and 10 iterations (solid line).

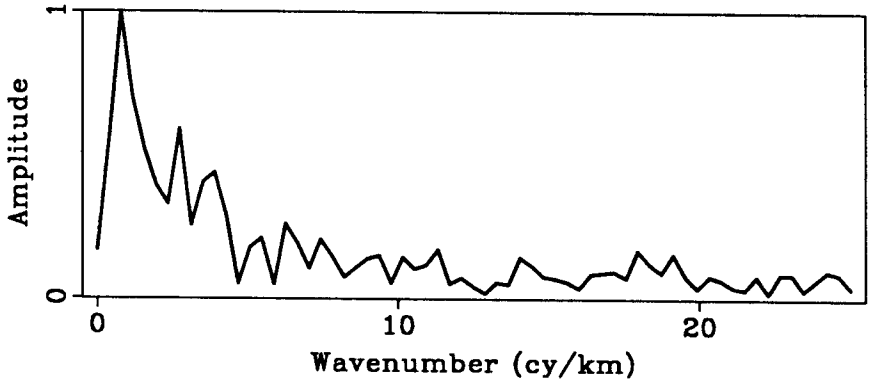

Figure 4.17: Vertical wavenumber spectrum of the true P-wave velocity log shown in Figure 4.15 (a).

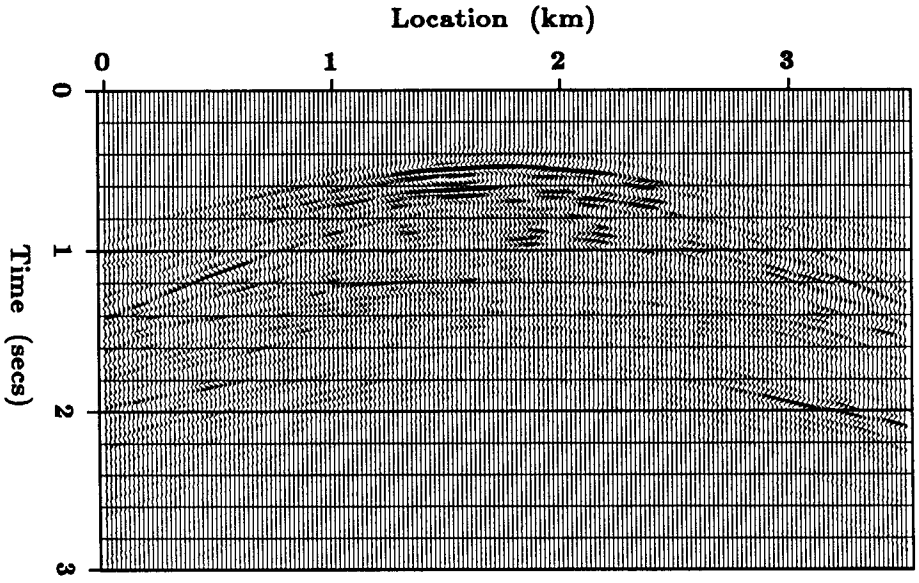

Figure 4.18: (a). Vertical component mismatch after ten iterations for the horst/reef example.

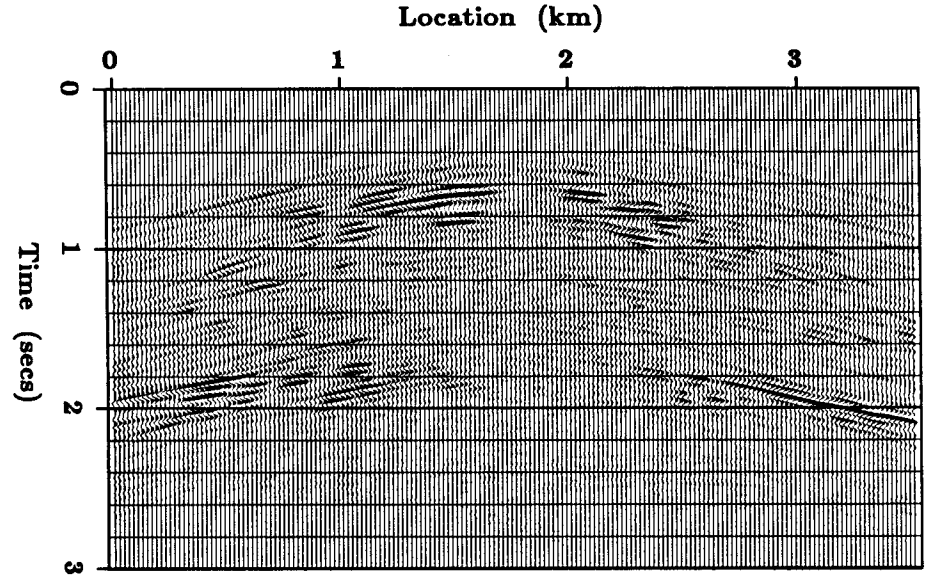

Figure 4.18: (b). Horizontal component mismatch after ten iterations for the horst/reef example.

The main point illustrated by these results is that my inversion can resolve between P- and S-wave velocities within the seismic bandwidth. By comparison, elastic migration is less capable of resolving between the two different velocities and does not yield absolute magnitudes of the velocity perturbations. Note that in reality, when the source strength is not well known, the absolute size of perturbations found in an inversion would be less reliable. The next chapter provides the key to the apparent problem of missing low wavenumbers in the inversion solution.

4.5 Transmission seismic data

This section shows that the inversion can be used for transmitted waves as well as reflected waves. Also, I wanted to study how the resolution is affected by the inclusion of transmitted waves. Transmitted waves, if present, are generally stronger than reflected waves so their influence should be larger. Also, considering their traveltime shape is greatly affected by the gross variations in velocity, I suspected that transmitted waves would help resolve the low wavenumbers in velocity just like traveltimes in a tomographic inversion.

This test used exactly the same parameters as the reflection data example except that some offset VSP's were included in the data set. Two-component VSP's were recorded down two wells on either side of the model for each of the nine shots. A representative VSP is shown in Figure 4.19.

The inversion result after one and ten iterations is shown in Figures 4.20 through 4.22. The ten iteration result is almost exactly the same as the true model that was used to generate the synthetic data. Both high and low wavenumbers of the P- and S-wave velocities have been well resolved. However, only the high wavenumbers of density were resolved. The low-wavenumber variations in density were not resolved indicating that they have little effect on the seismic waves (i.e. unlike low-wavenumber variations in velocity which strongly affect the traveltime, low-wavenumber density variations only affect the amplitude of the events but it appears that this amplitude variation may be easily attributed to other causes such as sudden velocity variations).

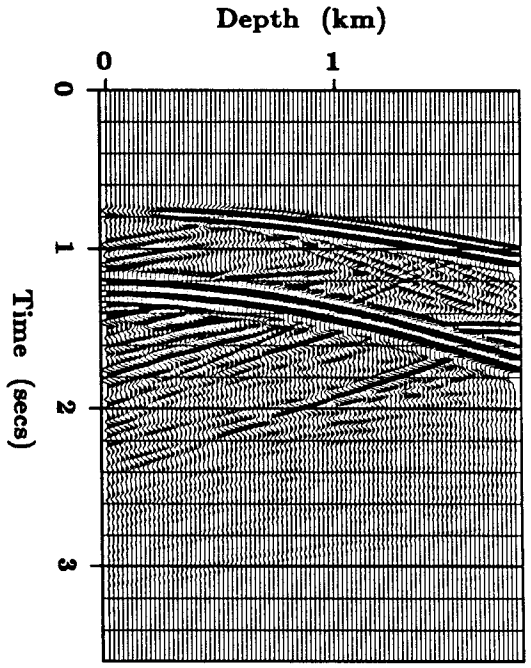

Figure 4.19: (a). A vertical component offset VSP for the horst/reef model.

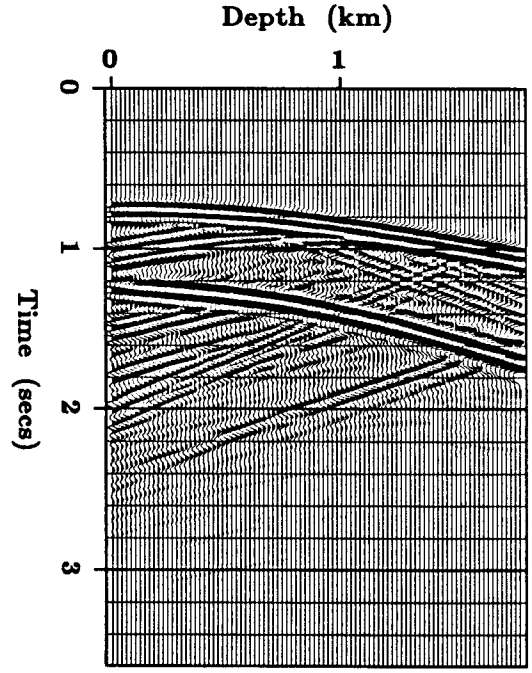

Figure 4.19: (b). A horizontal component offset VSP generated for the horst/reef model.

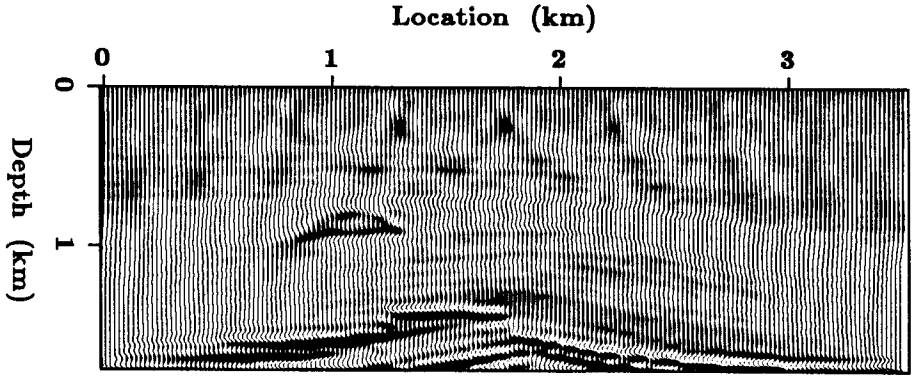

Figure 4.20: (a). One iteration P-wave velocity result using the horst/reef reflection and transmission data.

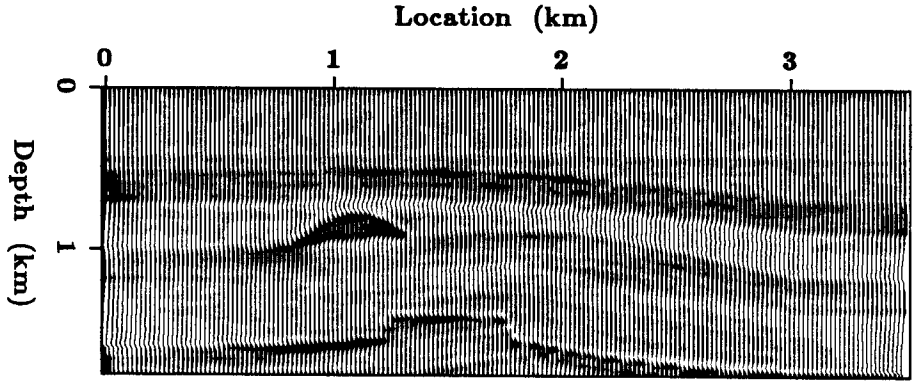

Figure 4.20: (b). Ten iteration P-wave velocity result using the horst/reef reflection and transmission data.

The velocity log through the reef (Figure 4.23) shows more quantitatively that the low wavenumbers were resolved. It is "blocky" (step-like) like the true model and the magnitudes of the perturbations are almost correct. The spectrum of this log is plotted in Figure 4.24. Unlike the spectrum for the reflection data inversion shown in Figure 4.16, this spectrum has a large predominance of low wavenumbers just like the true spectrum shown in 4.17.

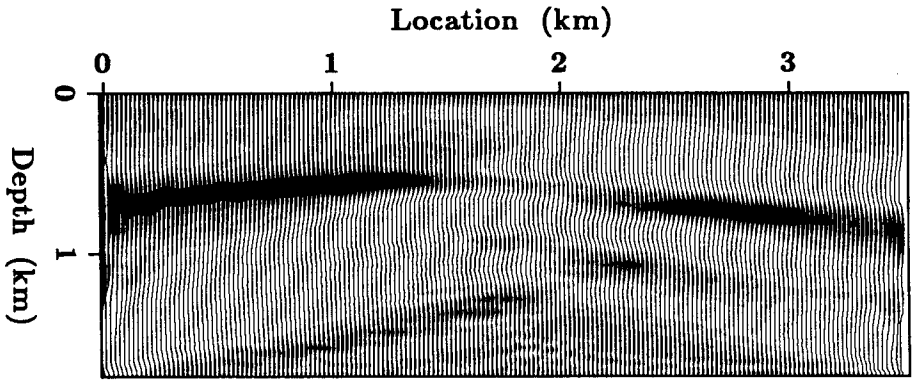

Figure 4.21: (a). One iteration S-wave velocity result using the horst/reef reflection and transmission data.

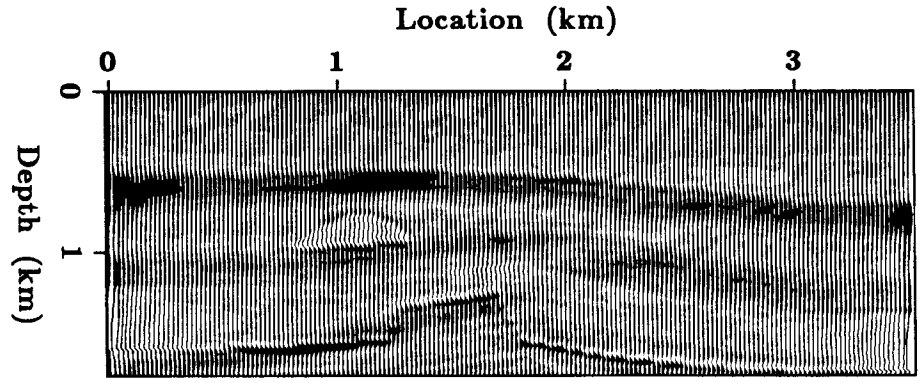

Figure 4.21: (b). Ten iteration S-wave velocity result using the horst/reef reflection and transmission data.

The square error sum decreases steadily as a function of iteration (Figure 4.25) indicating the algorithm is converging to a least-squares solution. The mismatch between the data computed from the ten iteration inversion result (termed the "synthetic data") and the synthetic data computed from the true model (termed the "true data") is shown in

Figure 4.26. It is mainly smaller than the usual noise level found in seismic data indicating that the algorithm has essentially converged. Because some significant mismatch remains in the transmitted waves, a few more iterations should further improve the low wavenumber velocity result.

Transmission data helps resolve the low wavenumber components of velocity so the inversion result looks "blocky" (step-like) like the true velocity model.

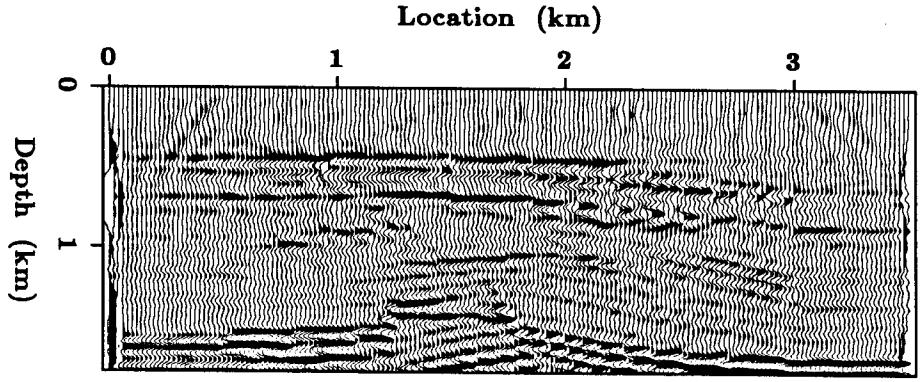

Figure 4.22: (a). One iteration density result using the horst/reef reflection and transmission data.

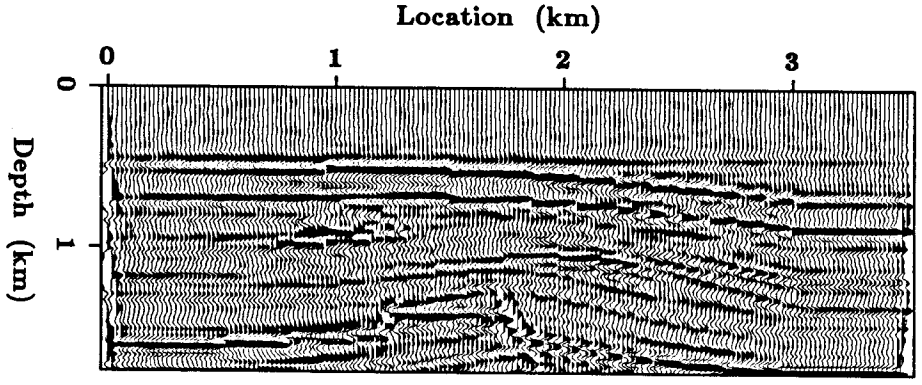

Figure 4.22: (b). Ten iteration density result using the horst/reef reflection and transmission data.

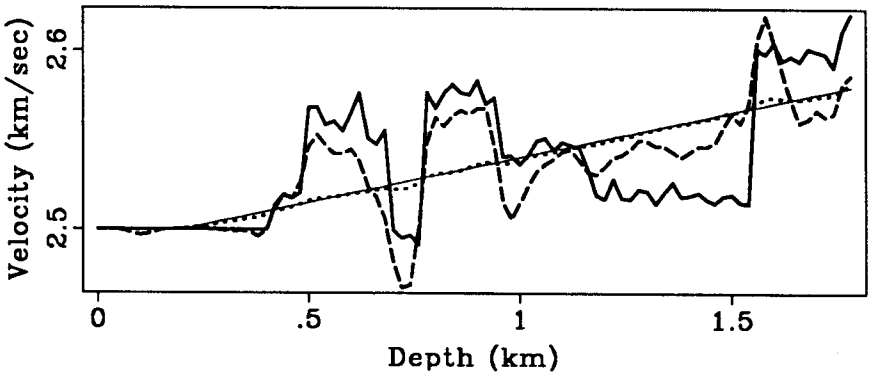

Figure 4.23: (a). P-wave velocity log through the reef: true model (bold line), initial model (fine line), one iteration result (dotted line) and ten iteration result (broken line).

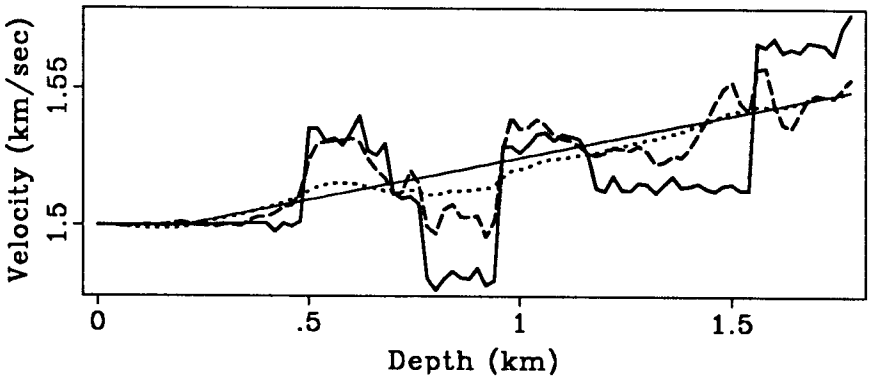

Figure 4.23: (b). S-wave velocity log through the reef: true model (bold line), initial model (fine line), one iteration result (dotted line) and ten iteration result (broken line).

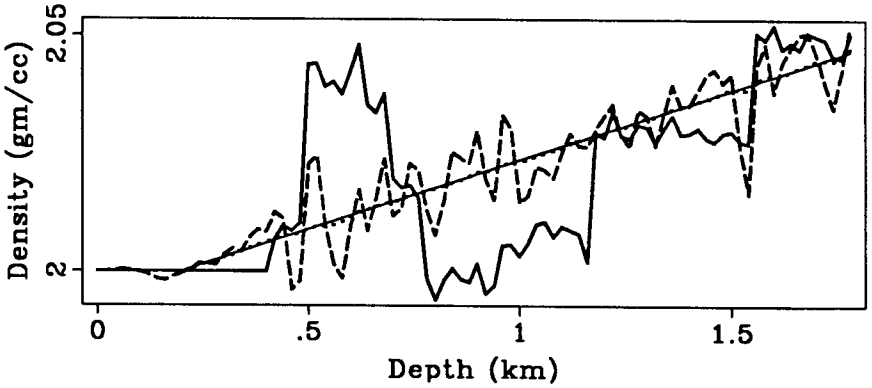

Figure 4.23: (c). Density log through the reef: true model (bold line), initial model (fine line), one iteration result (dotted line) and ten iteration result (broken line).

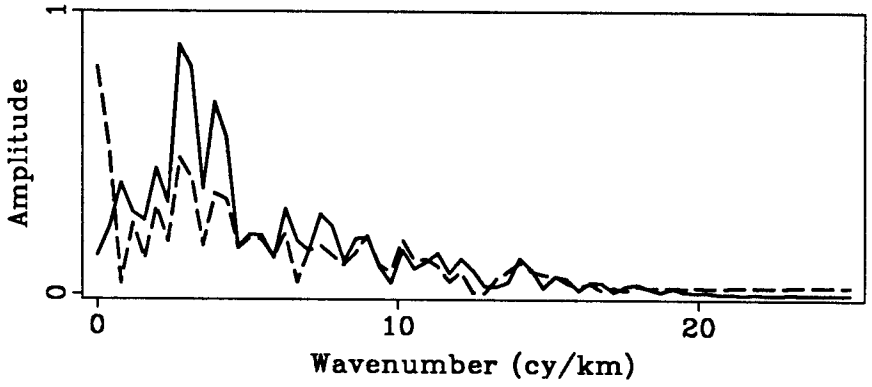

Figure 4.24: Vertical wavenumber spectrum of the P-wave velocity log through the reef obtained by the inversion shown in Figure 4.23 (a): after one iteration (broken line) and 10 iterations (solid line).

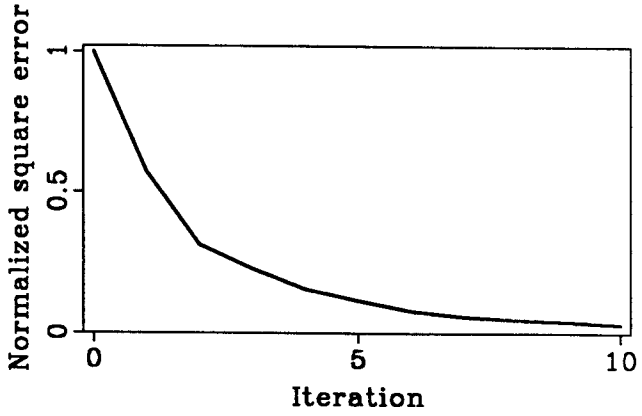

Figure 4.25: The normalized sum of the square error (misfit function) as a function of iteration number.

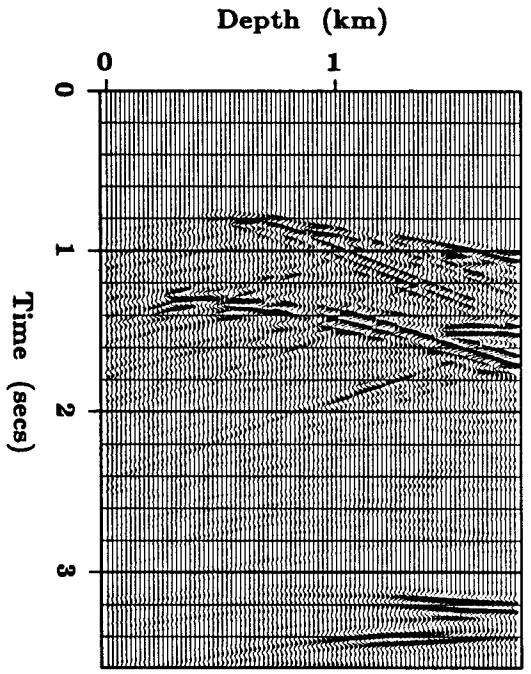

Figure 4.26: (a). Vertical component VSP mismatch after ten iterations for the horst/reef example.

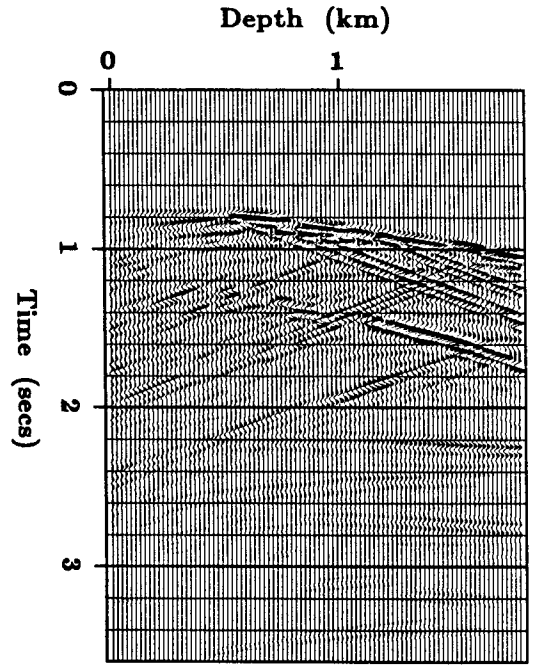

Figure 4.26: (b). Horizontal component VSP mismatch after ten iterations for the horst/reef example.

4.6 Field data

Field data presents the biggest challenge to any inversion technique because it may contain many factors not accounted for in the inverse theory. My inverse theory is based on the 2D isotropic elastic wave equation. Therefore, anisotropy and non wave-like effects, such as varying geophone couplings or machine noise, will be treated as noise. Inadequacies in converting the data from 3D to 2D will also influence the quality of the inversion. The conversion was done by applying a time varying gain of t to the field data which can be broken into a correction of $t^{.5}$ to convert from 3D to 2D for homogeneous velocity models plus an additional $t^{.5}$ correction to crudely allow for the additional divergence caused by the velocity increase with depth. Another factor is the source and receiver directivity patterns. Considering that rays at the Earth's surface are nearly vertical because of the low near-surface velocity, this directivity effect should be negligible (see also Appendix A).

Considering the long computation time, the field data inversion was restricted to the minimum number of shots (one) and iterations (a few = three) required to effectively demonstrate the method.

The two-component shot gather from a vertical vibrator source (chapter 2, Figure 2.1) was inverted. Note that this and the other shot gathers in this section are displayed with a t^2 gain.

Prior to the inversion, the missing central offsets were interpolated to decrease data truncation artifacts. Note that the interpolation consisted of NMO, dip-filtering of the steeper events and inverse NMO. This sequence interpolates events into the missing central offsets along hyperbolic trajectories. Furthermore, some of the noisy near-offset traces were replaced with the dip-filtered traces.

A velocity model obtained from a conventional velocity analysis was used as an initial guess in the iterative inversion (see Figure 2.3). Sharp discontinuities in interval velocity were present in this model. The synthetic data obtained by modeling using the initial model (Figure 2.2) was subtracted from the field data to obtain the mismatch at iteration zero (Figure 4.27). Note that no significant Rayleigh waves can be seen in the data so they were not included in the elastic finite difference modeling.

Three iterations of an inversion of the interpolated shot gather were performed. The mismatch after three iterations (Figure 4.28) is smaller than the mismatch at iteration zero so the algorithm was converging.

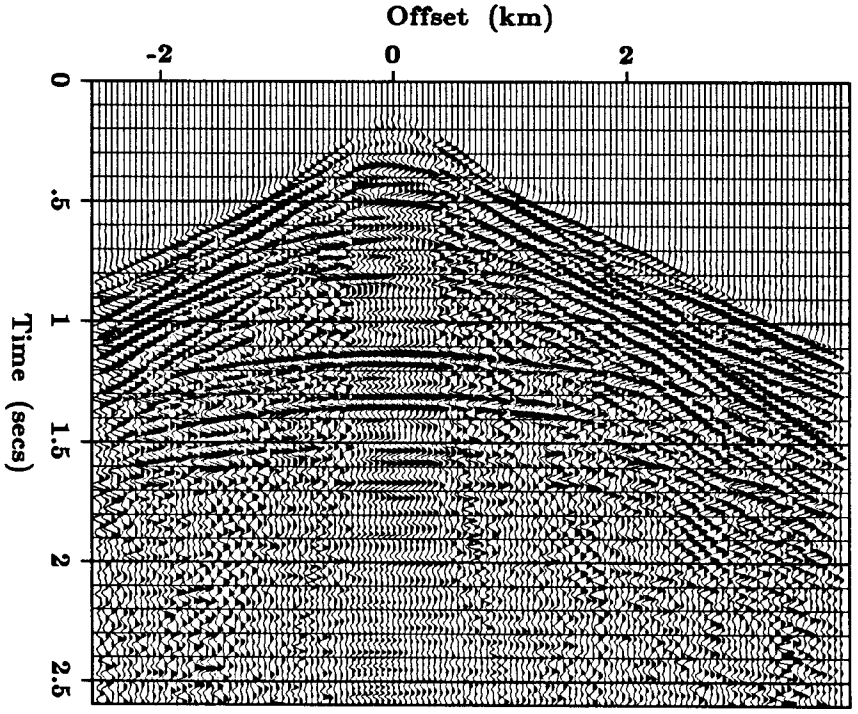

Figure 4.27: (a). Mismatch for the vertical-component field shot gather at iteration zero.

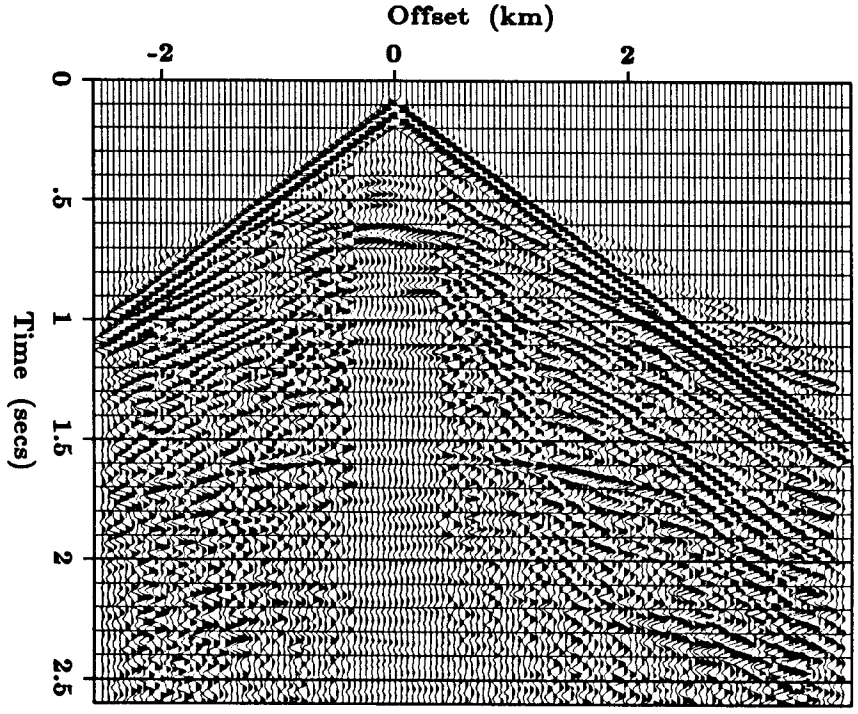

Figure 4.27: (b). Mismatch for the horizontal-component field shot gather at iteration zero.

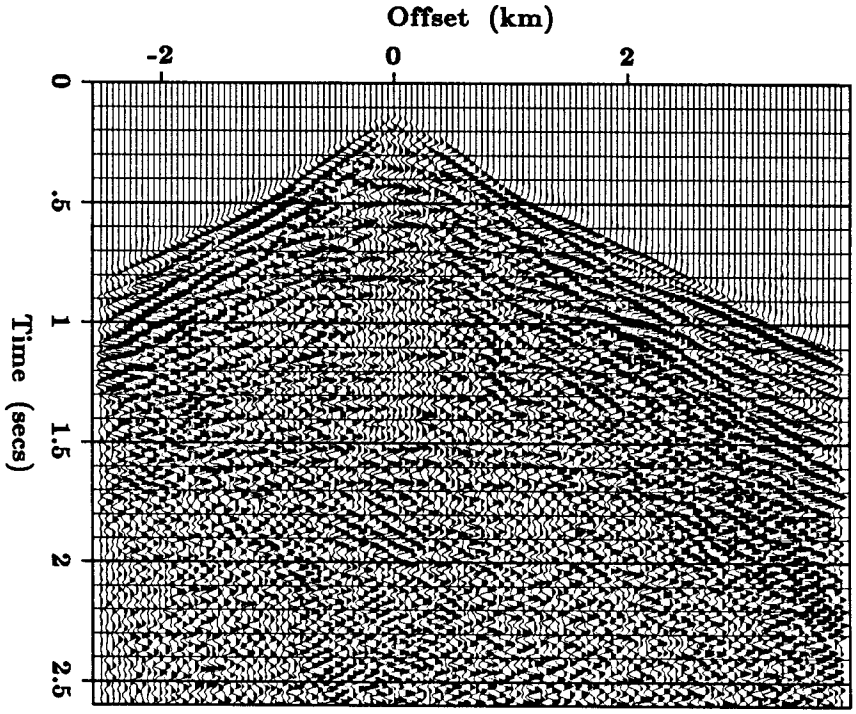

Figure 4.28: (a). Mismatch for the vertical-component field shot gather at iteration three.

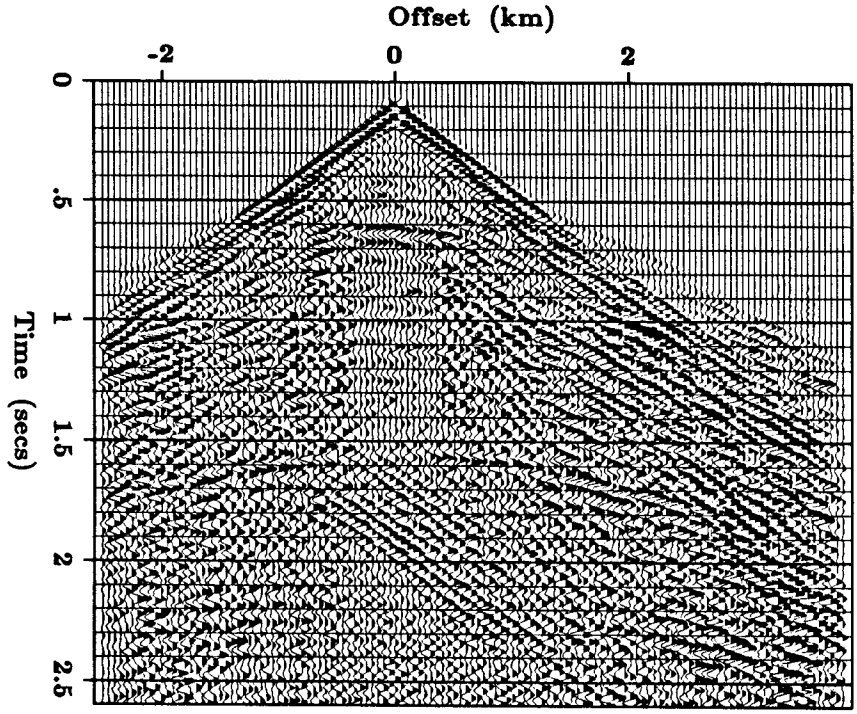

Figure 4.28: (b). Mismatch for the horizontal-component field shot gather at iteration three.

This can also be seen by observing that the normalized square error plotted in Figure 4.29 decreases as a function of iteration.

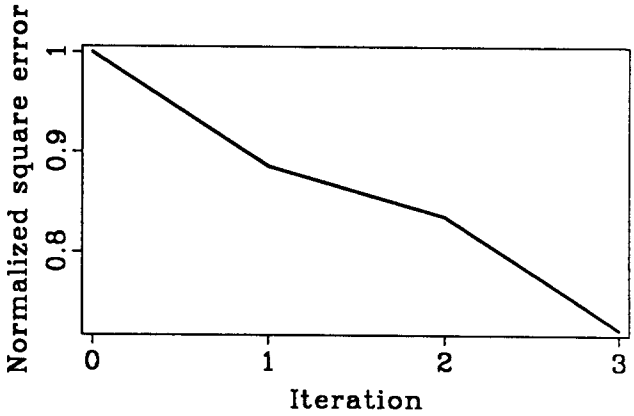

Figure 4.29: The normalized sum of the square error (misfit function) as a function of iteration number.

The inversion result is shown in Figure 4.30. Notice that the S-wave velocity is poorly resolved (noisier) directly below the shot because no mode converted waves passed through this region (the source was a vertical forcing function). An interesting feature in the P-wave velocity result is the smear to the right of the shot coming down in a semi-circular arc down to a reflector and back up to the shot. If many shots were included in the inversion, displaced circular arcs would be stacked together canceling everywhere except at depths around 1.0 km. Hence, an interval velocity perturbation is required at this depth to match the hyperbola shapes. This shows that the inversion algorithm resolves interval velocities as well as P- and S-wave reflectivities.

The results are good and do not contain excessive noise considering that the problem is not overdetermined (i.e. there are about the same number of model and data points).

Non-flat events in the images are correlations between P- and S-waves at non-geologic positions and are comparable to migration-smile artifacts. Synthetic studies shown earlier in this chapter indicated that the circular migration-smile-like artifacts tend to disappear after summing several shots and after several (about ten) iterations. Also, the signal to noise ratio in the solution increases as more shots are included and the problem becomes more overdetermined. Therefore, I expect that more complete and less noisy results could be obtained if more shot gathers were used and more iterations were done.

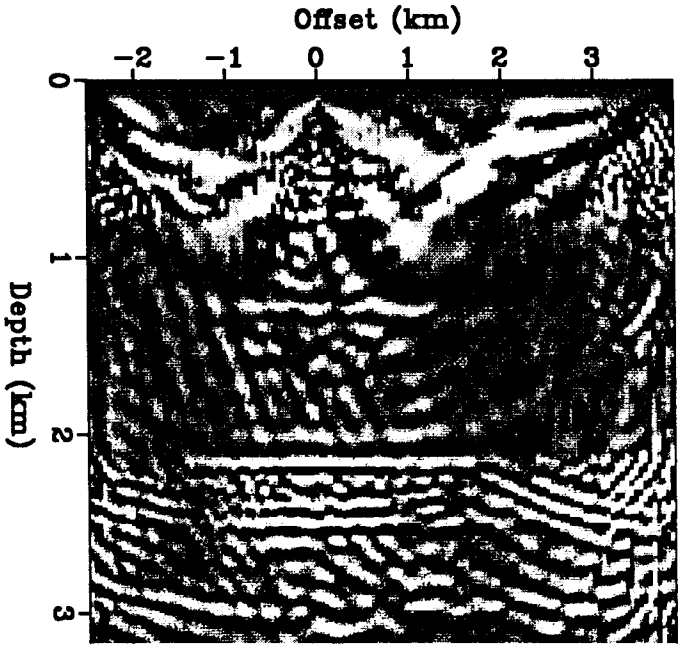

Figure 4.30: (a). Three iteration field data inversion result for compressional velocity.

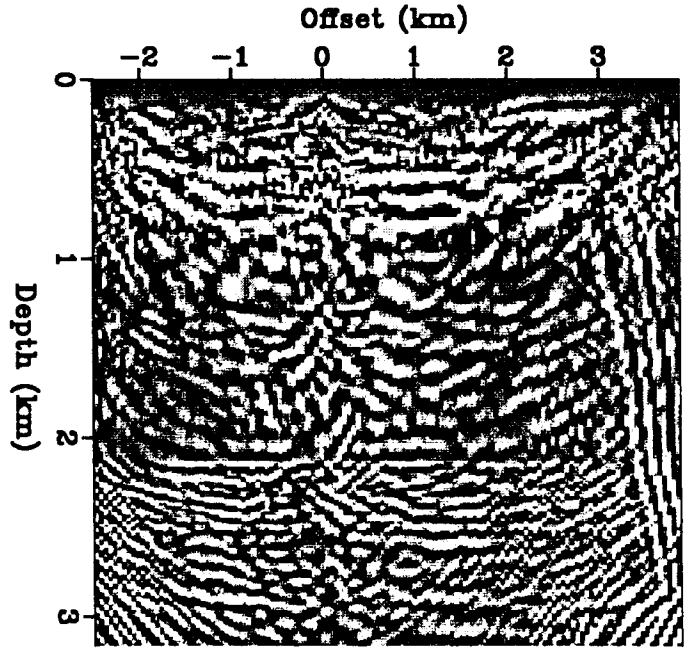

Figure 4.30: (b). Three iteration field data inversion result for shear velocity.

4.7 Conclusions

My inversion algorithm is capable of inverting seismic wavefields for the P- and S-wave velocities in the Earth provided the data contains P-P and P-S primaries. If the data contains transmitted waves (e.g. in VSP data), the inversion rapidly resolves the interval velocities. If only reflected waves are present (e.g. shot gathers), the sharp velocity perturbations across layer boundaries are resolved first. Reflection hyperbola shapes do help resolve the interval velocities but they converge slowly. However, there is some magic contained in the inversion formulas that enables the interval velocities to be resolved rapidly. The next chapter delves into this magic.